On the other hand, Hsu's team constructed a single chain incorporating the HR1 and HR2 peptide segments connected through an L6 linker (referred to as HR1–L6–HR2) and conducted a series of experiments to investigate its structure and stability. They observed the spontaneous assembly of this protein into a highly stable trimeric complex. Crystallographic analysis revealed a trimeric coiled-coil structure in the fusion core (**Fig. 3(a)**),[1] with specific residues involved in binding. The research team suggested that the fusion core of SARS-CoV-2 shares a similar conformation with those of other class I viruses, remarkably resembling the fusion core of SARS-CoV spike protein (**Fig. 3(b)**).[1] This indicates the possibility of employing similar methods to identify inhibitors effective against SARS-CoV-2 infection. Additionally, this structure provides crucial detailed information and target sites for structure-based drug design.

In summary, both studies elucidated the structural characteristics and biophysical properties of the RBD and fusion core. They noted that these features are essential in developing vaccines and therapeutic approaches for SARS-CoV-2 and other sarbecoviruses within the Coronaviridae family. (Reported by Chun-Hsiang Huang)

*This report features the work of Che Ma, Chun-Hua Hsu and their co-workers published in Nat. Commun. **14**, 311 (2023) and J. Chin. Chem. Soc. **70**, 1208 (2023).*

TPS 05A Protein Microcrystallography
TLS 15A1 Biopharmaceuticals Protein Crystallography
- XPS, Protein Crystallography
- Biological Macromolecules, Protein Structures, Life Science

References
1. C.-H Hsu, J. Chin. Chem. Soc. **70**, 1208 (2023).
2. K.-Y. A. Huang, X. Chen, A. Mohapatra, H. T. V. Nguyen, L. Schimanski, T. K. Tan, P. Rijal, S. K. Vester, R. A. Hills, M. Howarth, J. R. Keeffe, A. A. Cohen, L. M. Kakutani, Y.-M. Wu, M. Shahed-Al-Mahmud, Y.-C. Chou, P. J. Bjorkman, A. R. Townsend, C. Ma, Nat. Comum. **14**, 311 (2023).

Secrets of the Deadly Honeybee-Infecting Virus Unveiled

The atomic-resolution capsid structure of the honeybee-infecting virus could furnish valuable insights into the mechanisms governing viral capsid assembly, function, and infection with dynamic motions. This information can be harnessed for the development of natural drugs for honeybee colony protection.

Taiwan's warm temperatures, humid climate, and diverse array of nectar sources create a favorable environment for fostering honeybee habitats and promoting their propagation. Honeybees, in turn, play a crucial role in pollinating wild plants and agricultural crops. The two major honeybees, *Apis cerana Fabricius* (*A. cerana*) (Eastern honeybee) and *Apis mellifera Linnaeus* (*A. mellifera*) (Western honeybee) both play a crucial role in contributing to commercially valuable honey harvests and are both major honeybee species in the global beekeeping industry.[1] Colony collapse disorder (CCD) is a noteworthy phenomenon characterized by the sudden disappearance of as much as 90% of beehives in apiaries. Pathogens, including viruses, bacteria, fungi, mites, and environmental factors, such as chemical exposure and forage availability, have been identified as major contributors to disease in managed honeybee populations and are often associated with CCD.[2] Although the precise mechanisms of CCD remain elusive, evidence suggests that a newly discovered honeybee-infecting virus, Lake Sinai virus (LSV), plays a key role in this devastating disorder. The primary strains of LSV encompass two principal types, namely LSV1 and LSV2, along with other variants. LSV comprises a characteristic $T = 4$ quasi-equivalence nonenveloped capsid for packaging the single-stranded positive-sense RNA genome. The RNA genome size is ~5.6 kb and it encodes three major genes: Orf1 with unknown function, RNA-dependent RNA polymerase responsible for viral RNA replication, and the capsid protein (CP) for host recognition and viral capsid assembly. This work aims to explore the structures of LSV virus-like particles (VLPs), characterize all domain functions, and understand capsid assembly and RNA packaging during viral infection.

Although mature LSV virions are generally considered to exist solely in $T = 4$ assemblies, cryo-electron microscopy (cryo-EM) analyses of LSV2 and delta-N48 LSV1 VLPs uncovered structural polymorphism. By examining

approximately 11,000 particle images captured on an FEI Titan Krios microscope at Academia Sincia, Chun-Jung Chen (NSRRC) and his team determined the structures of LSV2 and delta-N48 LSV1 VLP capsids in both $T = 4$ and $T = 3$ architectures at resolutions of ~2.3 Å (**Fig. 1(a)**).[3] The external diameters of $T = 4$ and $T = 3$ LSV2 and delta-N48 LSV1 VLPs were found to be ~492 and 448 Å, respectively, with a protein shell thickness of ~100 Å at the widest points. The internal diameters of $T = 4$ and $T = 3$ LSV2 and delta-N48 LSV1 VLPs were ~294 and 250 Å, respectively (**Fig. 1(b)**). The X-ray diffraction and scattering data for both the crystal and solution structures of $T = 4$ and $T = 3$ LSV2 VLPs were acquired using the beamlines **TPS 05A** and **TPS 13A** at the NSRRC and **SP 44XU** at SPring-8.

The structures of $T = 4$ LSV2 and delta-N48 LSV1 VLPs are symmetrical icosahedral spheres exclusively comprising of 120 spikes on the outer surface and 240 copies of the 37-kDa full-length CP. In contrast, the $T = 3$ LSV2 and delta-N48 LSV1 VLPs consist of 90 spikes and 180 copies of CP. Extended spikes (3.6 nm in length) emanate from the center of each trimeric capsomere at the 3-fold axes. The *de novo* structural models for $T = 4$ and $T = 3$ LSV2 and delta-N48 LSV1 VLPs encompass all residues except for the N-terminal domain (NTD) and C-terminal domain (CTD), where no clearly defined density exists, implying flexibility or disorder (**Fig. 1(c)**). Specifically, the cryo-EM electron density maps of the protruding domain (P-domain) lack high-resolution details due to the absence of interpretable side-chain densities, suggesting a certain degree of flexibility at the outer capsid surfaces. Each subunit of the

$T = 4$ and $T = 3$ LSV2 and delta-N48 LSV1 VLPs adopts a folded structure consisting of several domains: the NTD, interior helical domain, central β-barrel domain, exterior P-domain, C-arm, and CTD. The central β-barrel domain of the LSV2 and delta-N48 LSV1 CPs incorporates a distinctive anchor loop, traversing the outer surface of the adjacent subunit with a clockwise rotation around the respective 3-fold axes (**Fig. 1(d)**).

The helical domain of the $T = 3$ delta-N48 LSV1 CP adopts a 3-fold helix similar to the LSV2 CP but is augmented by an additional N-terminal helix α1' that interacts with the core (α1, α11, and α12) of the helical domain. Moreover, focused refinement reconstruction of $T = 3$ delta-N48 LSV1 VLP provides a glimpse of RNA coordination, revealing a two-based single-strand RNA (ssRNA). Located on the inner surface of the capsid, the helix α1', α1'–α1 loop, and C-arm of delta-N48 LSV1 CP house several basic residues (9 arginines) within the inner cavity and play a functional role in viral nucleic-acid encapsidation.

To study the potential conformational states of the LSV VLP, the research team initially assessed VLP sizes and structures with cryo-EM under different pH conditions. Cryo-EM structures of both LSV2 and delta-N48 LSV1 VLPs were analyzed under neutral, acidic (pH 6.5), and alkaline (pH 8.5) pH conditions. The sizes of $T = 4$ and $T = 3$ LSV2 VLP particles depend on the pH, with diameters ranging from 494 to 482 Å and 450 to 438 Å, respectively, as conditions varied from alkaline to acidic (**Fig. 2(a)**). To obtain additional insights into the structural variations that
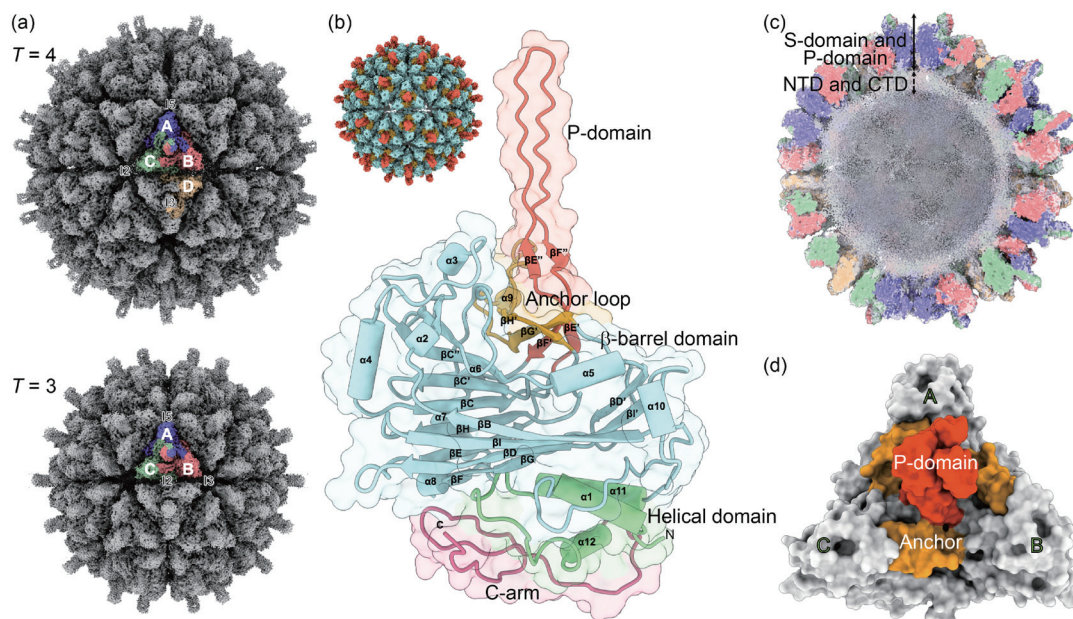

Fig. 1: (a) The comprehensive cryo-EM densities and configurations of $T = 4$ (upper) and $T = 3$ (lower) LSV2 VLPs, showcasing one icosahedral asymmetry unit, comprised of subunit A (purple), subunit B (red), subunit C (green), and subunit D (yellow, upper). (b) A structural depiction illustrating the modular arrangement of LSV2 capsid subunit A, encompassing the interior helical domain (green), the central β-barrel domain (cyan), the exterior P-domain (salmon red), the anchor loop (orange), and the C-arm (pink). (c) A cutaway view of the cryo-EM map for $T = 4$ LSV2 VLP, illustrating the P-domain, S-domain, NTD, and CTD. (d) Surface representation of a single homo-trimeric capsomere on the $T = 4$ LSV2 VLP. The P-domains are depicted in salmon red, and the anchor loops are presented in orange. [Reproduced from Ref. 3]
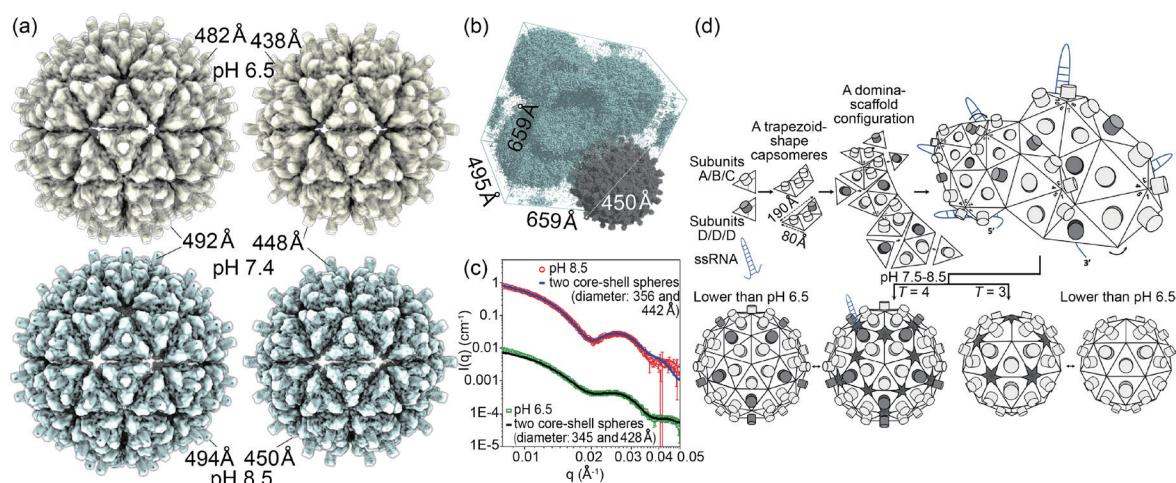
Fig. 2: (a) The cryo-EM maps illustrate $T = 4$ (left) and $T = 3$ (right) LSV2 VLPs with diameters of 482 and 438 Å, respectively, under acidic pH conditions, represented in dark khaki. Meanwhile, VLPs with respective diameters of 492 and 448 Å under neutral pH conditions are depicted in transparent rendering. (b) Molecular packing of the $T = 4$ LSV2 VLP in crystals is arranged in a unit cell with the space group $P4_2$. (c) The intensity vs. q profile of LSV2 VLPs as obtained from SAXS in different buffer solutions, with the buffer contribution subtracted. The $T = 4$ and $T = 3$ LSV2 VLPs, each with distinct particle sizes, are depicted in black and blue, respectively, under pH conditions of 8.5 and 6.5. (d) Schematic diagrams illustrating the presumed self-assembly mechanism of both $T = 4$ and $T = 3$ complete capsids of LSVs, highlighting the impact of pH conditions on the dynamic motion of VLP particles. The homo-trimeric capsomeres constitute a fundamental structural unit during the assembly process. [Reproduced from Ref. 3]

lead to pH-dependent particle size, the size fluctuations of $T = 4$ LSV2 VLP were examined using X-ray crystallography and small-angle X-ray scattering (SAXS). In the X-ray crystallographic analysis, the diameter of the $T = 4$ LSV2 VLP, measured to be 450 Å based on crystal packing, was marginally smaller than the size range identified by cryo-EM (**Fig. 2(b)**). During SAXS analysis, the pH conditions of LSV2 VLP were directly adjusted from pH 7.5 to pH 6.5 and 8.5. Conversely, the particle sizes of $T = 4$ and $T = 3$ LSV2 VLPs align closely with both the expanded and unexpanded conformations observed in the cryo-EM analyses (**Fig. 2(c)**). Interestingly, in many cryo-EM images of LSV2 VLP, linear structures comprising several trapezoid-shaped capsomeres arranged in a domino-like architecture were observed. This structural foundation of trapezoid-shaped capsomeres and the configuration resembling a domino scaffold offers insights into the mechanism of capsid assembly (**Fig. 2(d)**). Finally, mass spectrometry was used to characterize the autoproteolysis behavior of CP in a mutagenesis study, mimicking the cleavage site.

In summary, the atomic-resolution structures of LSV2 and delta-N48 LSV1 VLPs not only offer significant structural insights into viral capsids but also enable a detailed examination of the RNA-binding site and the driving forces behind capsid assembly. Despite the evolutionary and biological divergence of LSV, which has been classified into at least eight subgroups, many gene sequences of CP are conserved among strains of LSV. This study presents a structural model applicable to all strains of LSV, suggesting their self-assembly into common $T = 4$ tetravirus structures with single CP subunits and their ability to infect host cells

through a similar entry pathway. (Reported by Nai-Chi Chen)

This report features the work of Chun-Jung Chen and his collaborators published in Nat. Commun. 14, 545 (2023).

TPS 05A Protein Microcrystallography
SP 44XU Macromolecular Assemblies (International Collaboration)
- Protein Crystallography
- Biological Macromolecules, Protein Structures, Life Science
TPS 13A Biological Small-angle X-ray Scattering
- BioSAXS
- Structural Transitions of Macromolecules in Solution

References
1. D. Goulson, E. Nicholls, C. Botías, E. L. Rotheray, Science **347**, 1255957 (2015).
2. D. L. Cox-Foster, S. Conlan, E. C. Holmes, G. Palacios, J. D. Evans, N. A. Moran, P.-L. Quan, T. Briese, M. Hornig, D. M. Geiser, V. Martinson, D. vanEngelsdorp, A. L. Kalkstein, A. Drysdale, J. Hui, J. Zhai, L. Cui, S. K. Hutchison, J. F. Simons, M. Egholm J. S., Pettis, W. I. Lipkin, Science **318**, 283 (2007).
3. N. C. Chen, C. H. Wang, M. Yoshimura, Y. Q. Yeh, H. H. Guan, P. Chuankhayan, C. C. Lin, P. J. Lin, Y. C. Huang, S. Wakatsuki, M. C. Ho, C. J. Chen, Nat. Commun. **14**, 545 (2023).